4-5-2006

Electrochemical Performance of Co3O4–C Composite Anode Materials

Scott A. Needham
University of Wollongong, scottn@uow.edu.au

G. X. Wang
University of Wollongong, gwang@uow.edu.au

Konstantin Konstantinov
University of Wollongong, konstan@uow.edu.au

Y. Tournayre
University of Wollongong, yann@uow.edu.au

Z. Lao
University of Wollongong, zlao@uow.edu.au

See next page for additional authors

Electrochemical and Solid-State Letters, **9** (7) A315-A319 (2006)
1099-0062/2006/9(7)/A315/5/$20.00 © The Electrochemical Society

Electrochemical Performance of Co_3O_4–C Composite Anode Materials

S. A. Needham,[a,*,z] G. X. Wang,[b,] K. Konstantinov,[a] Y. Tournayre,[a] Z. Lao,[a] and H. K. Liu[b,**]**

[a]*Institute for Superconducting and Electronic Materials, Energy Materials Research Program, University of Wollongong, New South Wales 2522, Australia*
[b]*Institute for Superconducting and Electronic Materials, Australian Research Council Centre for Electromaterials Science, University of Wollongong, New South Wales 2522, Australia*

Co_3O_4–C composite powder has been synthesized via spray pyrolysis of cobalt nitrate-sugar solution at 600°C and assessed for application as anode materials in Li-ion batteries. Microstructural characterization by scanning electron microscopy, transmission electron microscopy, and energy-dispersive X-ray spectroscopy confirm an even distribution of carbon throughout particles, as well as the presence of a carbon-based surface sheath surrounding Co_3O_4–C particle agglomerates. Charge-discharge cycling of half-cells indicates a stable reversible discharge capacity above 800 mAh g^{-1}. Equivalent circuit modeling of Nyquist plots show the Co_3O_4–C electrode has significant kinetic advantages over non-composite transition metal oxide electrodes.
 [DOI: 10.1149/1.2197108]

Manuscript submitted December 14, 2005; revised manuscript received March 3, 2006. Available electronically May 4, 2006.

Poizot et al.[1] first reported that electrodes made of nanosized transition metal oxide (MO) particles (NiO, CoO, FeO, CuO, Cu_2O, and Co_3O_4) exhibit reversible capacities up to three times higher than electrodes composed of graphite. The most interesting aspect of this result is that these transition metal oxides do not display the classical hallmarks that have often been used by researchers to identify suitable Li-ion battery materials (i.e., reversible alloying with lithium or the existence of an open crystal framework). Rather, the reaction of these materials with Li^+ involves the thermodynamically unlikely reversible formation and decomposition of Li_2O.[2-7] Impetus for this reaction occurs through the formation of highly electrochemically reactive metal nanoparticles during cell discharge

$$M_xO_y + 2yLi^+ + 2ye^- \leftrightharpoons xM + yLi_2O \quad [1]$$

From all of the transition metal oxides studied, the Co_3O_4–Li system offers particular promise due to a reported reversible capacity in excess of 1000 mAh g^{-1}.[8] Unfortunately, the practical usage of Co_3O_4 cells in Li-ion batteries has been frustrated by capacity fade and a poor cycle life.[9,10] Part of these problems may be attributed to significant volume changes that occur during lithium uptake and removal (molar volume change ~100%) which may result in a loss of electrical contact and electrode failure. This situation is analogous to that found in tin-based oxides and alloys that also suffer significant volume changes.[11] Another important factor identified as influencing the cyclability of the Co_3O_4 electrode is the nature and electrochemical behavior of the solid electrolyte interphase (SEI). The SEI begins forming in the first discharge (reduction of MO) as a result of secondary reduction reactions within the electrolyte and has the appearance of a "polymer-like" gel.[6] Subsequent charging of the cell will often cause a partial dissolution of the SEI. The exact composition of the SEI obviously varies between systems and electrolytes, but the film is mildly conducting and is composed primarily of lithium-based carbonates and alkylcarbonates. This SEI formation-dissolution phenomenon that is caused by discharge-charge cycling of the cell is particularly influenced by the powder texture (crystallite and particle size, surface area, and surface composition) for each MO system. If precursor powders are too small, the SEI formation process dominates and cycle life of the cell is reduced. Specifically, smaller precursor MO powder particles will form more surface active metal nanoparticles during discharge, which are then available for catalytic reduction of the electrolyte and hence SEI formation. For example, work on nanosized Co_3O_4 precursor powders has shown that rapid SEI thickening caused by enhanced electrolyte degradation can occur to a point where Li transfer is significantly impeded and capacity fades.[12] Alternatively, work on Cu_2O cells that use larger microsized precursor MO powder have accredited an excellent capacity retention to the active formation-dissolution of the SEI.[2] Therefore, it is feasible that the SEI may be indirectly engineered by careful selection of the above characteristics to improve the cyclability of the transition MO electrode.

There has been a large amount of fundamental studies on the electrochemical performance of transition MOs that have focused on reaction mechanisms,[1,2,13] the development of possible intermediate phases,[14,15] and the effect of particle size on electrochemical performance.[14] However, to enhance the commercial viability of these materials and their application to large scale technology such as electric vehicles, practical improvements must be made in terms of capacity retention and cycle life. To this end, we have synthesized Co_3O_4–carbon (referred to as Co_3O_4–C hereafter) composite powders by chemical spray pyrolysis using common sugar (sucrose) as a carbon source. Sucrose is an attractive precursor to synthesize carbon because it is cheap, abundant, and has a high chemical purity. It has been shown that the confinement of MO clusters in a disordered carbon matrix can preserve electrical contact and cushion internal stresses, thereby leading to improved cycle life in a Li-ion cell.[16,17]

Experimental

Composite preparation.— Nanostructured Co_3O_4-C, Co_3O_4, and NiO powders were prepared in separate experiments using a vertical spray pyrolysis apparatus as described in our previous work.[18,19] The Co_3O_4 and NiO powders were obtained by spraying aqueous 0.2 M cobalt or nickel nitrate solutions at ambient temperature through an ultrasonic nozzle at 3 mL min^{-1} into an open air 2 m quartz tube at 600°C. For preparation of the Co_3O_4–C powder, the precursor solution contained 0.05 M sucrose and 0.2 M cobalt nitrate. The experimental conditions for pyrolysis of this solution were identical to those described for Co_3O_4 and NiO powders. All final powder products were confirmed by X-ray diffraction (XRD) to be reacted and usable as-received, however powders were dried overnight at 110°C in a vacuum oven to evaporate excess moisture prior to electrochemical testing.

Characterization.— Analysis of the composition and crystal structure of the powders was conducted using a Philips PW1730 X-ray diffractometer with monochromatized Cu Kα radiation (λ = 1.5418 Å) at a scan rate of 1° min^{-1}. The carbon content of the product Co_3O_4–C powder was analyzed by thermogravimetric (TG) method performed in static air on a Setaram 92 differential thermal analysis (DTA) apparatus at 10°C min^{-1}. An estimate of the crystallite sizes was calculated using the Scherrer equation: $D_{crystallite}$

* Elecrochemical Society Student Member.
** Elecrochemical Society Active Member.
z E-mail: scott_needham@uow.edu.au

$= 0.9\lambda/\beta \cos(\theta_B)$, where λ represents the X-ray wavelength, β is the observed full width at half-maximum (fwhm), and θ_B is the Bragg angle.[20] The morphology of the powders was observed by a JEOL JSM-6460A scanning electron microscope (SEM) and JEOL 2010 transmission electron microscope (TEM). The results obtained from TG experiment on Co_3O_4–C powder were compared to the carbon content calculated using an energy dispersive X-ray spectroscopy (EDXS) instrument attached to the abovementioned SEM. The specific surface area of the powders was calculated using the Brunauer, Emmett, Teller (BET) multipoint method with N_2 adsorbate at 77 K using a Quantachrome Nova 1000 Autosorb-1 gas sorption system.[21] Powders were weighed, placed in a Pyrex chamber, and outgassed at 140°C under inert gas flow for 1 h prior to measurement. Particle size distributions were determined using a Malvern Instruments Mastersizer.

Electrochemical assessment.— Electrochemical measurements were conducted by assembly of standard R2032 type coin cells. In the case of Co_3O_4 and NiO powders, working electrodes were constructed by mixing 80 wt % active powder, 8 wt % carbon black (Lexel, 99%), and 12 wt % polyvinylidene fluoride (Aldrich, 99%) in a mortar and pestle. For the Co_3O_4–C powder, 88 wt % of active material was used with the remaining 12 wt % made up of polyvinylidene fluoride binder. The dry powder mix was blended with *N*-methylpyrrolidinone to make a slurry, which was then spread uniformly on 1 cm^2 by 0.1 mm thick copper foil (99.99%) substrate. The electrodes were dried in a vacuum oven for 12 h at 80°C then cold pressed at 300 kg cm^{-2} in a uniaxial hydraulic press. All electrodes contained no more than 2 mg of active material and were assembled into a test coin cell in a high purity argon-filled glove box (Mbraun, Unilab, USA) where the concentration of $H_2O < 5$ ppm and $O_2 < 10$ ppm. Battery grade lithium foil was used as both the counter and reference electrodes. Celgard 2400 was used as a separator membrane soaked in 1 M $LiPF_6$ dissolved in a 1:1 (vol:vol) mixture of ethylene carbonate (EC) and dimethyl carbonate (DMC) electrolyte (Merck KgaA, Germany). Charge-discharge cycles of the half-cells were measured between 0.02 and 3.0 V vs lithium at the C/30 rate using a Neware battery cycler in galvanostatic mode. Specific capacity was calculated based on the mass of active material in the electrode and all electrochemical testing was carried out at ambient temperature (23 ± 2°C). Electrochemical impedance spectroscopy (EIS) measurements were conducted using a CH Instruments electrochemical workstation (CHI 660A). The impedance spectra were recorded potentiostatically by applying an ac voltage of 5 mV at various open-circuit voltages (OCVs) on the tenth discharge. Simulation of impedance spectra with an equivalent circuit was performed over identical frequency range using Zview computer software (Version 2.8, Scribner Associates, USA). The program fits the parameters of the equivalent circuit of each of the electrodes using the complex nonlinear least squares (CNLS) method, which provides simultaneous fits for each parameter. Note that the electrodes used for the impedance analysis had a uniform film thickness in the 60–70 μm range to allow a valid comparison of impedance values.

Results and Discussion

Figure 1 shows the XRD patterns for the sprayed Co_3O_4–C, Co_3O_4, and NiO powders. The diffraction patterns seen in Fig. 1a are indexed to the cubic Co_3O_4 phase with $Fd\bar{3}m$ space group (JPDD ICDD reference 65-3103). Crystallite sizes for the Co_3O_4–C and Co_3O_4 powders were calculated using the Scherrer equation at 10.2 and 12.0 nm, respectively. The swollen nature of the Co_3O_4–C graph at low scattering angle ($2\theta < 30°$) is indicative of disordered carbon.[22,23] The diffraction pattern in Fig. 1b shows Bragg reflections indexed according to pure phase NiO bunsenite compound with cubic crystal structure and $Fm\bar{3}m$ space group (JPDD ICDD reference 01-1239). The broadened nature of the three main diffraction peaks at 37.4, 43.5, and 62.6° [(111), (200), and (220) reflections, respectively] suggests that the powder has a nanocrystalline

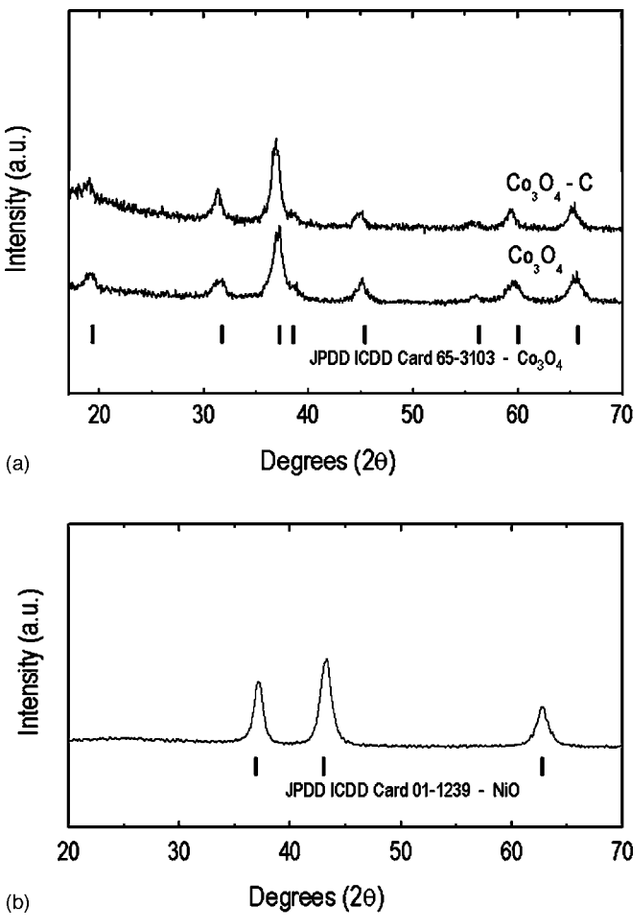

Figure 1. XRD patterns of (a) Co_3O_4–C, Co_3O_4 and (b) NiO powders.

morphology, which is confirmed by a calculated crystallite size of 8.7 nm. Dark field TEM analysis (data not shown) supports that the crystallite sizes for all powders are of the magnitude calculated empirically.

The actual quantity of carbon in the Co_3O_4–C composite powder was calculated by TG analysis at 22 wt % and EDXS area analysis at 27 wt %. The close agreement of these values confirms that the C content of the composite to be in the 20–30 wt % range. It is expected that a large fraction of the carbon in the precursor solution was also lost to the atmosphere as CO_2 during pyrolysis, and can be explained by considering the behavior of sucrose upon heating. When sucrose is hydrolyzed, it first decomposes into its two smaller monosaccharide isostructural constituents, namely, glucose and fructose (Reaction 2).[24] Slow heating initiates a series of up to 25 sequential reactions occur whereby different classes of compounds are formed including aldehydes, ketones, carboxylic acids.[25] However, regardless of heating rate there are two main exothermic reactions of decomposition that occur before 600°C and involve the formation of large quantities of CO_2, H_2O (Reaction 3), and carbon (Reaction 4)

$$C_{12}H_{22}O_{11} + H_2O \rightarrow 2C_6H_{12}O_6 \quad [2]$$

$$C_6H_{12}O_6 + 6\ O_2 \rightarrow 6CO_2 + 6H_2O \quad [3]$$

$$C_6H_{12}O_6 \rightarrow 6C + 6H_2O \quad [4]$$

Figure 2 shows SEM and TEM images of the as-prepared Co_3O_4–C powder at different magnifications. Figure 2a shows a low magnification SEM of the morphology of the Co_3O_4–C powder. The majority of particles measure less than 5 μm and consist of a mix-

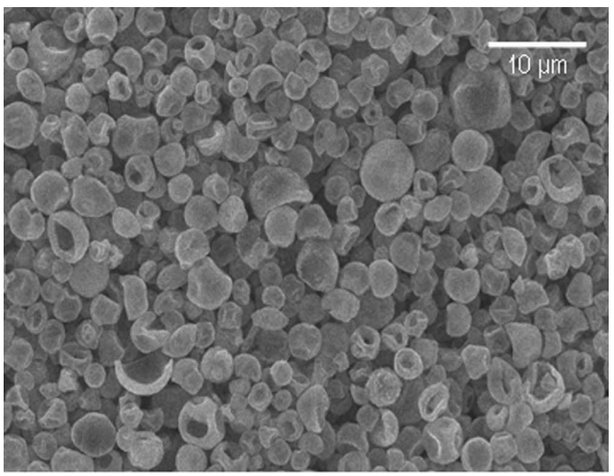

(a)

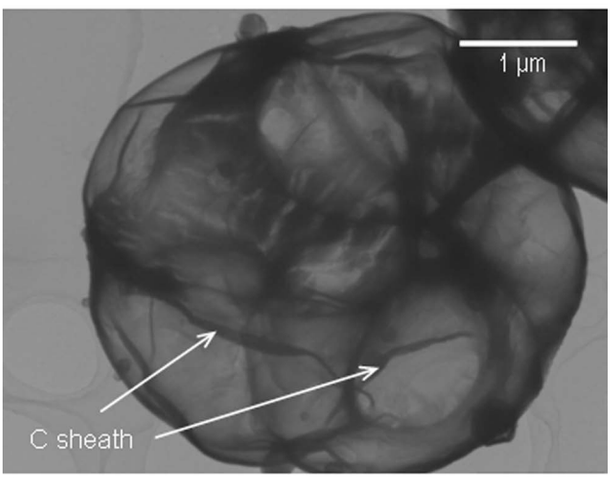

(b)

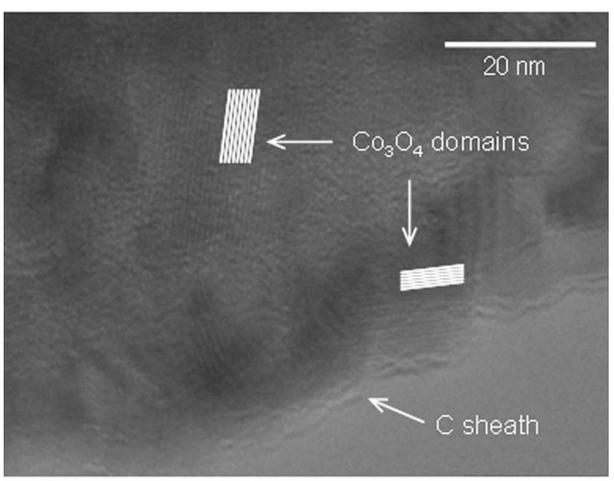

(c)

Figure 2. Images of Co_3O_4–C powder showing (a) a low magnification SEM view, (b) TEM of the nanoporous carbon sheath coated on a Co_3O_4–C particle, (c) and a TEM image of finely distributed disordered C and crystalline Co_3O_4 domains within an individual particle.

ture of partially and fully developed hollow spheres, with the average wall thickness of 0.5–2 μm. EDXS analysis indicates that carbon is evenly distributed across the surface of Co_3O_4–C particles

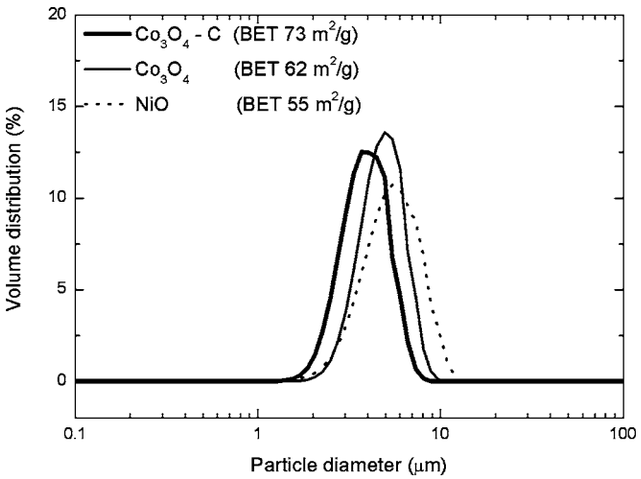

Figure 3. Particle size distribution and BET specific surface areas of Co_3O_4–C, Co_3O_4, and NiO powders.

and also throughout the wall thickness. The TEM image in Fig. 2b shows that each particle visible in Fig. 2a is actually an agglomeration of sub-micrometer Co_3O_4–C particles coated in a thin C-rich sheath, with the composition of the surface layer being confirmed by selected area electron diffraction (SAED). It is thought that this type of morphology may form as a result of the highly reactive particles coalescing within the reaction chamber, moments after being sprayed. The thickness of the C sheath is 2–5 nm and can be seen in Fig. 2c coating grains containing a fine distribution of disordered carbon (black spots <1 nm) and domains of crystalline Co_3O_4.

Figure 3 shows the particle size distribution and BET surface areas of Co_3O_4–C, Co_3O_4, and NiO powders. All powders show a narrow Gaussian distribution from 2 to 10 μm that supports SEM observations. The surface area of powders in decreasing order was Co_3O_4–C (73 $m^2\ g^{-1}$), Co_3O_4 (62 $m^2\ g^{-1}$), and NiO (55 $m^2\ g^{-1}$). The higher surface area measured in Co_3O_4–C is explained by the additional gases given off during processing that have resulted in an aerated powder product. Small angle X-ray scattering (SAX) experiments conducted in other works[26] have indicated that pyrolyzed carbons contain a mix of open and closed nanopores that can significantly increase the powder surface area. In these studies, a maximum surface area was achieved at spray temperatures 600–700°C, which corresponds well with the processing temperature used in our present study. From an electrochemical performance viewpoint, the higher surface area measured in Co_3O_4–C powder implies that more electrolyte could be exposed to the particle surface. It is well documented that although this may produce initial improvements in the cell capacity, the electrode capacity can rapidly fade upon cycling due to the accelerated degradation of the electrolyte and concomitant formation of a thick SEI layer that surrounds active particles.[3,12] However, as seen in Fig. 4, the Co_3O_4–C electrode demonstrated superior electrochemical performance compared to Co_3O_4 and NiO electrodes. In Fig. 4a, the Co_3O_4–C electrode maintains a capacity >800 mAh g^{-1} for 50 cycles, whereas Co_3O_4 and NiO electrodes show a steady decay to 300 and 280 mAh g^{-1} respectively. Indeed, the Co_3O_4–C electrode also demonstrates better capacity retention than Co_3O_4 electrodes that were prepared by thermal decomposition of a cobalt octacarbonyl compound and reported by our group elsewhere.[9,10] The first and fiftieth cycle discharge curves for electrodes made from Co_3O_4–C, Co_3O_4, and NiO powders is shown in Fig. 4b. Here we see the voltage plateaus that were present for the noncomposite Co_3O_4 (at 1.1 V) and NiO (at 0.6 V) during the first cycle, almost disappear in the fiftieth cycle. Conversely for the Co_3O_4–C electrode, the voltage plateau that was responsible for the high capacity achieved in early cycling is pre-

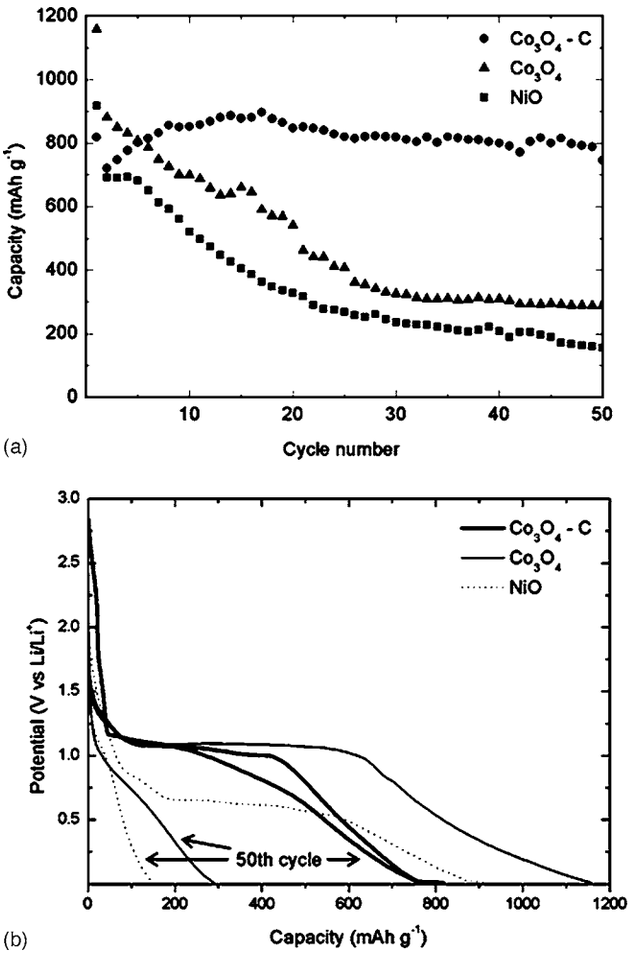

Figure 4. Comparison of electrochemical performance for Co_3O_4–C, Co_3O_4, and NiO electrodes showing discharge capacity over (a) 50 cycles and the (b) first and fiftieth cycle discharge curves.

served in the fiftieth cycle. We believe that part of the reason for the improved cyclability may be attributed to carbon coating on the surface of Co_3O_4 crystals. We expect that this coating could simultaneously shield electrolytes from advanced decomposition caused by exposure to Co nanoparticles, enhance the overall electronic conductivity of the electrode, and also provide a cushion effect to accommodate volume expansion and contraction during discharge-charge cycling.[11] Furthermore, any volume changes upon cycling may also be partially accommodated by the fine distribution of disordered carbon present throughout the bulk powder.

EIS was used to further elucidate the nature of the cyclability improvement demonstrated in the Co_3O_4–C electrode, by collecting Nyquist plots at various predetermined voltages (2.0, 1.6, 1.2, 1.0, 0.8, 0.4, and 0.2 V) on the tenth discharge cycle. Impedance spectra were recorded by applying an ac voltage of 5 mV amplitude over the frequency range 100 kHz to 10 mHz, after a 2 h rest at each potential to attain equilibrium. EIS is a powerful technique for Li-ion electrode kinetic analysis due to the information that can be deduced for each reaction process; concerning that of the electrolyte, passivation layer(s), charge transfer, and Li^+ diffusion. The impedance spectra on 10th discharge for Co_3O_4–C and Co_3O_4 electrodes at various OCV are presented in Fig. 5. For all measurements, the overall shape of Nyquist plots show the characteristic depressed semicircle in the high and middle-frequency range and an extended tail at ~45° to the Z' axis. The semicircle is often considered to be the superposition of two individual semicircles, even though the

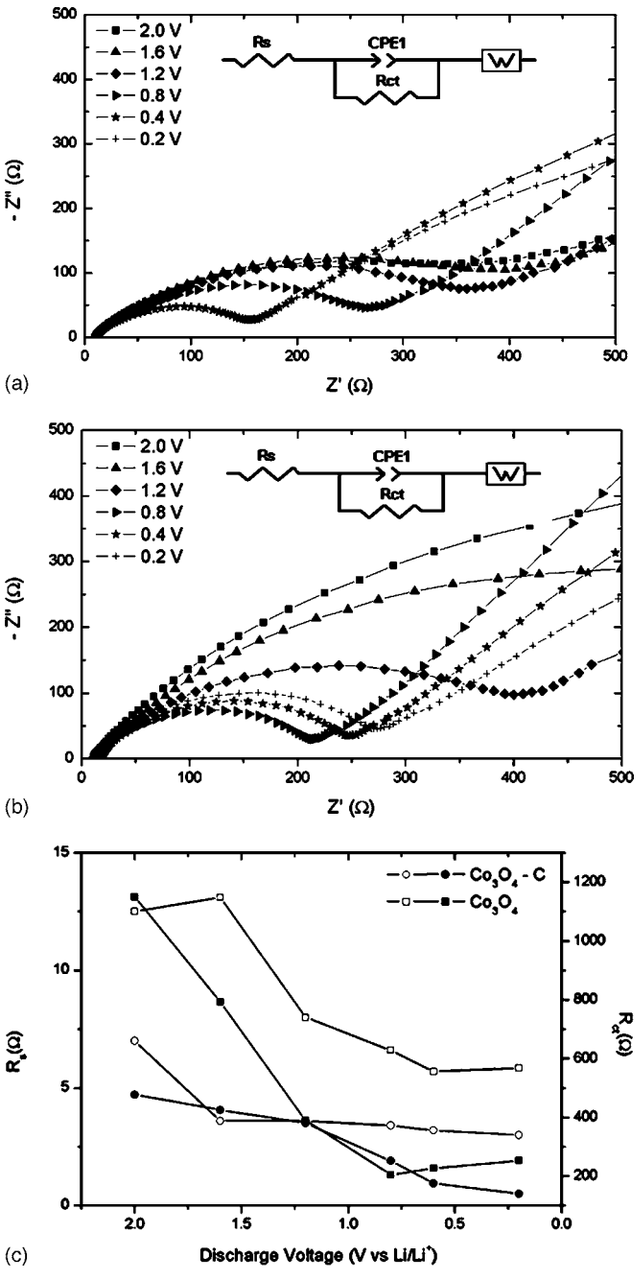

Figure 5. Nyquist plots of (a) Co_3O_4–C and (b) Co_3O_4 electrodes and (c) scatter plots of various equivalent circuit parameters vs discharge voltage. R_s is represented by open symbols and R_{ct} by closed symbols.

exact separation of these is not well developed in our case. Usually, a small, high-frequency semicircle is identified that corresponds to the formation of a passivated film (SEI) and creates impedance at the surface of the working electrode particles in contact with the organic electrolyte.[27-29] The resistance (R) and capacitance (C) values associated with the migration of Li^+ through the SEI are described by Eq. 5 and 6

$$R = \rho l/S \quad [5]$$

$$C = \epsilon S/l \quad [6]$$

where S is the electrode surface area and l is the thickness, ρ is the resistivity, and ϵ the permittivity of the SEI layer.[30] However, because only one semicircle is distinguishable, the exact contribution

to impedance of this component is difficult to quantify.[31] The semicircle that dominates at intermediate frequency represents the charge transfer impedance (R_{ct}) through the electrode–electrolyte interface, and is considered to account for a large proportion of the overall kinetic impedance of the cell. From Fig. 5a and b, the size of this semicircle in both electrodes reduced considerably at voltages lower than 1.2 V since the primary reaction plateau for $Co_3O_4 + 8Li^+ + 8e^- \rightarrow 3Co + 4Li_2O$ occurs at just below this value. The sloping line at $\sim 45°$ to the Z' axis found at low frequency is known as Warburg impedance and is representative of diffusion of Li^+ within the bulk anode.[32] The high frequency intercept at the Z' axis corresponds primarily to the electrolyte resistance (R_s), however small contributions may exist from the wire resistance of the system and solid-solid contact.

To obtain quantitative results, an equivalent circuit (insets of Fig. 5a and b) was used to fit the Nyquist plots where R_s=solution resistance, R_{ct}=charge transfer resistance, and W is the Li^+ diffusion resistance. A constant phase element (CPE_1) was used to account for the complexity of the double layer effect associated with charge transfer resistance. The fit result parameters are summarized in Fig. 5c where we see R_s values for the Co_3O_4–C electrode are lower than those of the Co_3O_4 electrode. The values of R_{ct} at various potentials also show the same trend, except at 0.8 and 1.2 V where the values are similar. We attribute the generally lower trend of values of R_s and R_{ct} for the Co_3O_4–C electrode to the improvement of electronic conductivity due to the formation of a disordered carbon sheath. Moreover, the sheath that coats Co_3O_4 crystals in the Co_3O_4–C composite could also induce the formation of a high quality stable SEI layer, thereby contributing to the excellent cycling performance.[27]

Conclusions

We have produced nanocrystalline Co_3O_4–C composite powder by spray pyrolysis technique that has a narrow Gaussian type particle size distribution (2–10 μm) and high specific surface area (73 $m^2\ g^{-1}$). Preliminary electrochemical testing of Co_3O_4–C electrodes indicates a high reversible capacity of 800 mAh g^{-1}, whereas the noncomposite Co_3O_4 and NiO electrodes show a steady decay upon cycling to less than 40% of their original capacity. By synthesizing Co_3O_4–C powders we have overcome rapid capacity fade often associated with finely divided Co_3O_4 powder. The formation of a C sheath on the particle surface can potentially shield the catalytic action of the Co nanoparticles on electrolyte reduction and the retard development of a thick SEI that can impede charge transfer. In addition, we expect that the disordered C matrix throughout the bulk powder and the carbon sheath assist to cushion the volume expansion associated with the reversible formation of Co nanoparticles. It can be assumed that these results are not limited to the Co_3O_4 system but also to other promising transition MO–C composite powders.

Acknowledgments

The authors acknowledge financial support provided by the Australian Research Council (ARC) through ARC linkage project LP0453766 and the Centre of Excellence program.

The University of Wollongong assisted in meeting the publication costs of this article.

References

1. P. Poizot, S. Laruelle, S. Grugeon, L. Dupont, and J.-M. Tarascon, *Nature (London)*, **407**, 496 (2000).
2. S. Grugeon, S. Laruelle, R. Herrera-Urbina, L. Dupont, P. Poizot, and J.-M. Tarascon, *J. Electrochem. Soc.*, **148**, A285 (2001).
3. P. A. Connor and J. T. S. Irvine, *Electrochim. Acta*, **47**, 2885 (2002).
4. W.-Y. Li, L.-N. Xu, and J. Chen, *Adv. Funct. Mater.*, **15**, 851 (2005).
5. V. Pralong, J. B. Leriche, B. Beaudoin, E. Naudin, M. Morcrette, and J.-M. Tarascon, *Solid State Ionics*, **166**, 295 (2004).
6. S. Laurelle, S. Grugeon, P. Poizot, M. Dolle, L. Dupont, and J.-M. Tarascon, *J. Electrochem. Soc.*, **149**, A627 (2002).
7. P. Poizot, S. Laurelle, S. Grugeon, L. Dupont, and J.-M. Tarascon, *J. Power Sources*, **97**, 235 (2001).
8. Y. Wang, Z.-W. Fu, and Q.-Z. Qin, *Thin Solid Films*, **441**, 19 (2003).
9. G. X. Wang, Y. Chen, K. Konstantinov, J. Yao, J.-H. Ahn, H. K. Liu, and S. X. Dou, *J. Alloys Compd.*, **340**, L5 (2002).
10. Y. Chen, G. X. Wang, K. Kostantinov, J. H. Ahn, H. K. Liu, and S. X. Dou, *J. Metastable Nanocryst. Mater.*, **15–16**, 625 (2003).
11. S. A. Needham, G. X. Wang, and H. K. Liu, *J. Alloys Compd.*, **400**, 234 (2005).
12. Z. Yuan, F. Huang, C. Feng, J. Sun, and Y. Zhou, *Mater. Chem. Phys.*, **79**, 1-4 (2003).
13. Z.-W. Fu, Y. Wang, Y. Zhang, and Q.-Z. Qin, *Solid State Ionics*, **170**, 105 (2004).
14. D. Larcher, G. Sudant, J.-B. Leriche, Y. Chabre, and J.-M. Tarascon, *J. Electrochem. Soc.*, **149**, A234 (2002).
15. M. M. Thackery, S. D. Backer, and K. T. Adendorff, *Solid State Ionics*, **17**, 175 (1985).
16. H. Li, L. Shi, W. Lu, X. Huang, and L. Chen, *J. Electrochem. Soc.*, **148**, A915 (2001).
17. H. Li, X. J. Huang, and L. Q. Chen, Z. G. Wu, and Y. Liang, *Electrochem. Solid-State Lett.*, **2**, 547 (1999).
18. K. Konstantinov, J. Wang, S. Bewlay, G. X. Wang, H. K. Liu, S. X. Dou, and J.-H. Ahn, *J. Metastable Nanocryst. Mater.*, **15-16**, 325 (2003).
19. Z. W. Zhao, K. Konstantinov, L. Yuan, H. K. Liu, and S. X. Dou, *J. Nanosci. Nanotechnol.*, **4**, 861 (2004).
20. P. Scherrer, *Nachr. Ges. Wiss. Goettingen, Math.-Phys. Kl.*, **2**, 98 (1918).
21. S. Brunauer, P. H. Emmett, and E. Teller, *J. Am. Chem. Soc.*, **60**, 309 (1938).
22. W. Xing, J. S. Xue, and J. R. Dahn, *J. Electrochem. Soc.*, **143**, 3046 (1996).
23. W. Xing, R. A. Dunlap, and J. R. Dahn, *J. Electrochem. Soc.*, **145**, 62 (1998).
24. R. Owusu-Apenten, *Introduction to Food Chemistry*, p. 51, CRC Press, Boca Raton, FL (2004).
25. P. M. Gaman and K. B. Sherrington, *The Science of Food: An Introduction to Food Science, Nutrition, and Microbiology*, p. 52, Pergamon Press, New York (1981).
26. A. Gibaud, J. S. Xue, and J. R. Dahn, *Carbon*, **34**, 499 (1996).
27. D. Aurbach, *J. Power Sources*, **89**, 206 (2000).
28. D. Aurbach and A. Zaban, *J. Electrochem. Soc.*, **141**, 1808 (1994).
29. M. D. Levi and D. Aurbach, *J. Phys. Chem. B*, **101**, 4630 (1997).
30. M. Dolle, F. Orsini, A. S. Gozdz, and J.-M. Tarascon, *J. Electrochem. Soc.*, **148**, A851 (2001).
31. W.-R. Liu, J.-H. Wang, H.-C. Wu, D.-T. Shieh, M.-H. Yang, and N.-L. Wu, *J. Electrochem. Soc.*, **152**, A1719 (2005).
32. I.-S. Kim, G. E Blomgren, and P. N. Kumta, *J. Electrochem. Soc.*, **152**, A248 (2005).